Ultralow-frequency Raman system down to 10 cm^{-1} with longpass edge filters and its application to the interface coupling in t(2+2)LGs

M.-L. Lin,[1] F.-R. Ran,[2] X.-F. Qiao,[1] J.-B. Wu,[1] W. Shi,[1] Z.-H. Zhang,[3] X.-Z. Xu,[3] K.-H. Liu,[3] H. Li,[2] and P.-H. Tan[1,a)]

[1]*State Key Laboratory of Superlattices and Microstructures, Institute of Semiconductors, Chinese Academy of Sciences, Beijing 100083, China*

[2]*Key Laboratory of Flexible Electronics (KLOFE) & Institute of Advanced Materials (IAM), Jiangsu National Synergetic Innovation Center for Advanced Materials (SICAM), Nanjing Tech University (NanjingTech), 30 South Puzhu Road, Nanjing 211816, China*

[3]*School of Physics, Center for Nanochemistry, Collaborative Innovation Center of Quantum Matter, Peking University, Beijing 100871, China*

(Received 3 March 2016; accepted 9 May 2016; published online 27 May 2016)

Ultralow-frequency (ULF) Raman spectroscopy becomes increasingly important in the area of two-dimensional (2D) layered materials; however, such measurement usually requires expensive and nonstandard equipment. Here, the measurement of ULF Raman signal down to 10 cm^{-1} has been realized with high throughput by combining a kind of longpass edge filters with a single monochromator, which are verified by the Raman spectrum of L-cystine using three laser excitations. Fine adjustment of the angle of incident laser beam from normal of the longpass edge filters and selection of polarization geometry are demonstrated how to probe ULF Raman signal with high signal-to-noise. Davydov splitting of the shear mode in twisted (2+2) layer graphenes (t(2+2)LG) has been observed by such system in both exfoliated and transferred samples. We provide a direct evidence of twist-angle dependent softening of the shear coupling in t(2+2)LG, while the layer-breathing coupling at twisted interfaces is found to be almost identical to that in bulk graphite. This suggests that the exfoliation and transferring techniques are enough good to make a good 2D heterostructures to demonstrate potential device application. This Raman system will be potentially applied to the research field of ULF Raman spectroscopy. *Published by AIP Publishing.* [http://dx.doi.org/10.1063/1.4952384]

I. INTRODUCTION

Ultralow-frequency (ULF) Raman spectroscopy with signal detection ranging from 5 cm^{-1} to 100 cm^{-1} relative to the laser excitation line has been used to investigate the fundamental vibrational properties in various objects and materials. For instance, it has been applied to explore so called "boson" vibration peaks in glasses in the terahertz range (5-100 cm^{-1}),[1,2] acoustic phonons in nanocrystals[3,4] and nanorods,[5,6] folded acoustic phonons in semiconductor superlattices,[7,8] the shear (C) modes, layer-breathing (LB) modes, and thus the interlayer coupling in two-dimensional (2D) layered materials, such as graphene and transition metal dichalcogenides layered materials.[9–11] Also, ULF Raman signals are becoming more and more important to identify the thickness and the stacking order of various 2D layered materials and heterostructures.[10–23] However, due to the technical restrictions, the explorations of ULF Raman modes are still limited. On the one hand, the Rayleigh scattering signal is up to 12 orders of magnitude higher than the Raman signal. On the other hand, ULF Raman modes is very close to the laser line. From a practical point of view, (i) the laser line must be as monochromatic as possible, (ii) the Rayleigh signal must be effectively attenuated to make ULF Raman signal be detectable from the Rayleigh background, and (iii) the throughput of Raman signal should be as high as possible to improve the signal-to-noise ratio.

In order to access ULF Raman signal, several techniques have been applied to confocal Raman system. The standard apparatus to access Raman signal in the ULF region is double or three cascaded high-resolution monochromators, which provide flexible operations down to 5-10 cm^{-1} at different wavelengths.[7,24] However, the throughput of this setup is at least one-order of magnitude lower than a single monochromator, resulting long accumulated time. Recently, ULF Raman signal can be obtained with BragGrate™ notch filters (BNFs) based on volume Bragg grating (VBG) techniques.[9] The narrow bandwidth (around 10 cm^{-1}) and high transmittance (up to 80%-90% dependent on the laser wavelength) for each filter make it possible to measure ULF Raman modes with easy operation by a single monochromator. However, in order to effectively reject Rayleigh signal, 3-4 BNFs are usually used. The narrow bandwidth of BNFs and complicated configuration lead to inconvenience in the system adjustment and high cost, complexity to realize ULF Raman measurement for each laser wavelength. Therefore, a compact Raman system with high throughput and easy operation is desirable and necessary in the ULF Raman spectroscopy.

Here, a configuration of Raman system based on a single monochromator with a kind of longpass edge filter is introduced. Using such Raman system, ULF Raman modes can be detected down to 10 cm^{-1} with high throughput and easy operation. The Raman system has been verified by measuring

a)Electronic mail: phtan@semi.ac.cn

ULF modes in Ge/Si quantum dot superlattices (QDSLs) and L-cystine. We apply this setup to probe the interface shear (C) and layer-breathing (LB) coupling in two twisted (2+2) layer graphenes (t(2+2)LG) prepared by exfoliation and transferring, respectively. The LB coupling at twisted interfaces in t(2+2)LG is almost identical to that in Bernal-stacked bilayer graphene (2LG) while the shear coupling is significantly softened at twisted interfaces. We provide a direct evidence of twist-angle dependent softening of the shear coupling in twisted multilayer graphenes.

II. INSTRUMENTATION AND PERFORMANCE

A home-modified commercial Jobin-Yvon HR800 spectrometer was used as a single monochromator system for ULF Raman measurement. The spectrometer is equipped with a liquid-nitrogen-cooled CCD, a 100× objective lens (numerical aperture = 0.90), and several gratings. The excitation wavelengths are 488 nm from an Ar^+ laser, 532 nm from a diode-pumped solid-state laser, 633 nm from a He-Ne laser, and 785 nm from a Ti:Saphire laser. The resolution of the Raman system at 2.54 eV is ~0.6 cm^{-1} per CCD pixel. A Nano-Edge type of longpass edge filters (Nano-edge filters) from Iridian Corp was used to align the optical path and achieve ULF Raman measurement. Nano-edge filters offer cut-offs of less than 0.2% of the laser wavelength, high transmittance (>90%), low ripple (<4%-5%), and deep blocking (>OD 6) at the laser line. For comparison purposes, we used a RU-type of normal longpass edge filter (RU-edge filter) from Semrock Corp and four BNFs from OptiGrate Corp for the 532 nm excitation. Only Stokes Raman signals can be detected by the longpass Nano-edge and RU-edge filters because anti-Stokes Raman signals are blocked by these filters. A tungsten halogen lamp was used for the transmittance measurement of optical filters. The typical laser power is ~0.5 mW, to avoid sample heating.

The experimental setup integrated with BragGrate band-pass filter (BPF), Nano-edge filter, and a single monochromator are showed in Fig. 1. BPF is used to remove plasma lines

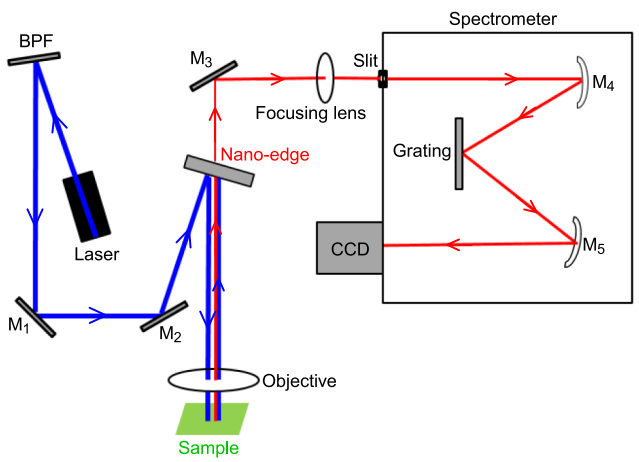

FIG. 1. Schematic diagram for ultralow-frequency (ULF) Raman configuration with Nano-edge filters and BPF, where at least 5 mirrors are necessary and denoted as M_j, j = 1, 2, 3, 4, and 5.

of the lasers. BPF is based on volume Bragg grating technique whose spectral widths can be as small as 5-10 cm^{-1}. Because BPF is a reflecting filter, at least two mirrors are necessary to align the laser excitation to the center of Nano-edge filters and precisely adjust the incident angle to Nano-edge. The Nano-edge filters are placed on a filter holder with two adjustment screws so that one can align the laser beam reflected by Nano-edge filters to the microscope objective. Combining with the two mirrors and adjustable filter holder, one can tune the angle between incident laser beam and the normal of Nano-edge filters in order to gain the best laser line attenuation and ULF Raman signal with frequency as low as possible. Two pieces of Nano-edge filters are used to reach deep blocking at the laser line up to OD 12. The high transmittance of Nano-edge filters makes the Raman signals in the ULF region effectively and selectively be guided into the single monochromator. The Nano-edge filters in Fig. 1 can be changed into two pieces of RU-edge filters for comparison purposes. The configuration of BNFs for ULF Raman measurement can be found in Ref. 9.

We first measured the transmittance of the three Raman filters, i.e., BNFs, Nano-edge filters, and RU-edge filters, at the wavelength of 532 nm, as show in Fig. 2(a). The transition width of BNF, Nano-edge filters, and RU-edge filters is 5, 10, and 120 cm^{-1}, respectively. This allows the lowest wavenumber detected by each filters, as depicted in Fig. 2(b) for the Ge/Si QDSL. Because the signal throughput of each BNF at 532 nm is about 75%, 4 BNFs will result in a signal throughput of 35%, which is much lower than 76% of the two Nano-edge filters. The superlattice of the QDSL makes the longitudinal acoustic modes of bulk Si be folded into the center of the Brillouin zone (BZ) and forms the folded longitudinal acoustic (FLA) modes. The unit cell of the QDSL is so large that the wavevector at the BZ edge can be comparable to the photon vector.[7] The selection rule of momentum conservation in Raman scattering makes FLA modes be observable and series of FLA modes appears in the Raman spectra, as shown in Fig. 2(b). The 1st order FLA modes at 4.2 and 5.8 cm^{-1} were detected by 4 BNFs, while we detected the 2nd order FLA modes at 14.4 and 16.1 cm^{-1} by Nano-edge filters, which are consistent with the corresponding transition width in the transmittance spectra of BNF and Nano-edge filters. Although the standard cut-off for a 532-nm Nano-edge filter is 38 cm^{-1}, the detectable Raman signal can be down to 10 cm^{-1} by two Nano-edge filters after the fine adjustment of their working angle. Because of the limit of transition width up to 120 cm^{-1} for RU-edge filters, no FLA modes can be detected by RU-edge filters. It should be noted that the intensity of the FLA modes detected by BNFs is less than half of that by Nano-edge filters because of much high signal throughput in Nano-edge filters as addressed above.

In order to test the effect of polarized geometries on ULF Raman measurement, Fig. 2(c) shows Raman spectra of L-cystine using 532, 633, and 785 nm excitations and the corresponding Nano-edge filters under both parallel (VV) and cross (HV) polarization geometries. In a polarization geometry of "XY," the former "X" indicates the polarization direction of laser beam while the latter "Y" is that of Raman signal. We found that the setup with the HV geometry can record

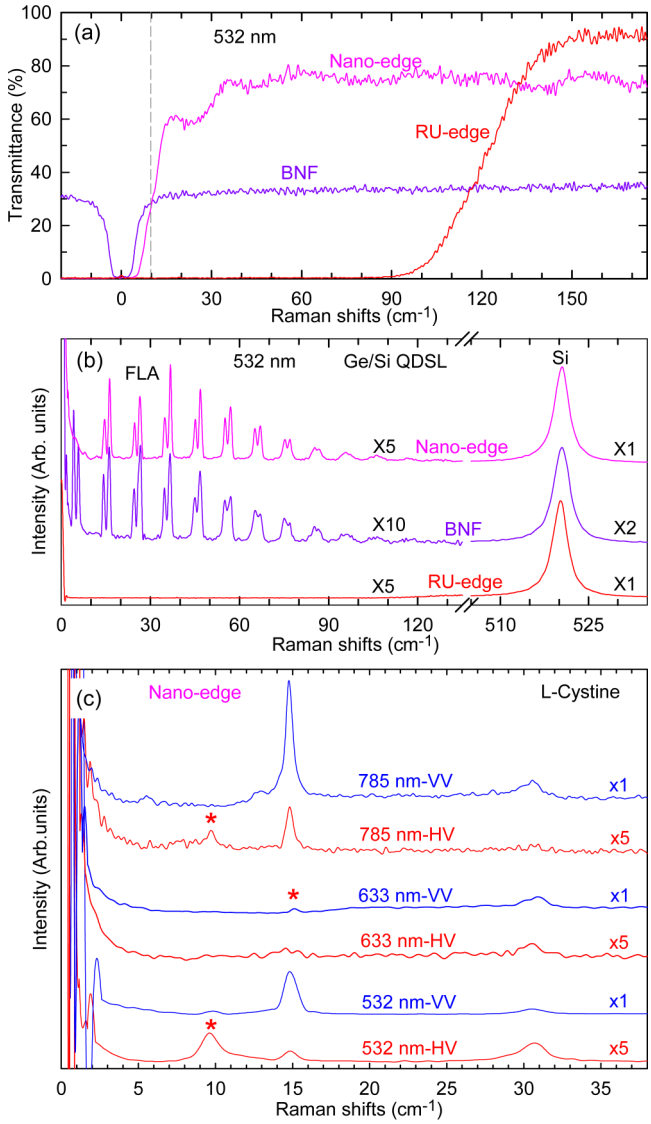

FIG. 2. (a) Optical transmittance of BNFs, Nano-edge filters, and RU-edge filters at 532 nm; (b) Stokes Raman spectra of the FLA and Si modes of the Ge/Si QDSL measured by the three types of Raman filters and 532 nm laser excitation. The spectra are scaled and offset for clarity. (c) Raman spectra of L-cystine powder in the parallel (VV) and cross (HV) geometries for three excitations: 785 nm, 633 nm, and 532 nm.

ULF Raman signals with lower frequency than that with the VV geometry. The lowest cut-off wavenumber in the HV geometry can reach as low as about 8 and 10 cm^{-1} for 532 and 785 nm excitations while 15 cm^{-1} for 633 nm, respectively, as indicated in Fig. 2(c) by stars. The detection limit of each Nano-edge filter in the ULF range is determined by its cut-off and steepness. In the HV geometry, the second polarizer can serve as another filter to attenuate the Rayleigh scattering signal which is usually with the same polarization as the laser beam. This is why a triple grating spectrometer can be used to detect ULF Raman signal down to 15 cm^{-1} in cross polarized geometry while it is not the case in unpolarized geometry.[25] Therefore, the HV geometry can be used in a single monochromator with edge filters to probe Raman modes with lower frequency once they are Raman active in such geometry.

Most applications call for optical filters to be used at normal incidence. However, for Raman measurement, the configuration in Fig. 1 is preferred in which Raman filters can be used as a mirror to reflect the laser beam to the sample and simultaneously as an attenuator to block the Rayleigh line in the Raman signal. For a fixed laser power, maximum Raman intensity can be obtained in such configuration. In Fig. 1, the angle of incidence (AOI) of the incident laser from normal of Raman filters is always non-zero. Therefore, it is important to understand how the spectral properties of Nano-edge filters (also most kinds of optical filters) change when using these filters at a non-normal AOI. There are two main effects exhibited by all filter spectrum as AOI is increased from normal: (1) The features of the spectrum shift to shorter wavelengths (i.e., toward anti-Stokes side); (2) Two distinct spectra emerge—one for *s*-polarized light and one for *p*-polarized light. For the Raman signal excited by a laser beam with V polarization, *s*-polarized and *p*-polarized components can be measured in VV and VH geometries, respectively. If no polarizer is used for Raman signal, the geometry corresponds to V(V+H). Fig. 3 presents the optical transmittance of Nano-edge filters for 633 nm with different AOIs and the corresponding Stokes FLA modes of the Ge/Si QDSL in V(V+H) and HH geometries. Indeed, with increasing AOI, *s*-polarized and *p*-polarized components are separated in the transmittance spectra of Nano-edge filters, as indicated in Figs. 3(a)-3(c). AOI in Fig. 3(a) is close to zero. With increasing AOI, the cut-off band of Nano-edge filters shifts

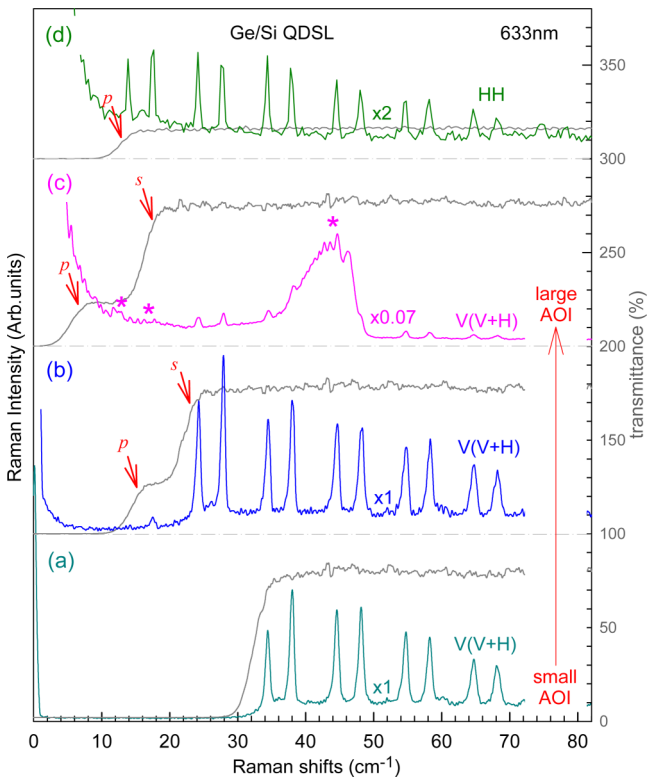

FIG. 3. Optical transmittance of Nano-edge filters for 633 nm and the corresponding Stokes Raman signals of the Ge/Si QDSL with different AOIs from normal of Nano-edge filters in the V(V+H) geometry ((a)-(c)) and in the HH geometry (d). All the transmittance and Raman spectra are scaled and offset for clarity.

to lower frequency for both *s*-polarized and *p*-polarized components, and thus lower Raman signals can be probed. *p*-polarized component exhibits lower cut-off frequency than *s*-polarized component. However, once Rayleigh signal cannot be efficiently blocked by the edge of *p*-polarized band of Nano-edge filters, the Rayleigh signal will become saturated at the ULF region and result in some additional ghost peaks (e.g., signals labeled by stars in Fig. 3(c)) in this region, which significantly reduce the signal-to-noise of Raman signal. *If one further increase AOI, Nano-edge filters cannot block Rayleigh signal anymore and CCD may be damaged by the intense Rayleigh signal.* Therefore, fine adjustment of Nano-edge filters is very important to optimize the AOI of Nano-edge filters and to detect ULF Raman signal with high signal-to-noise. In the HH polarization geometry, ULF mode can be detected down to 10 cm^{-1} in the Ge/Si QDSL with fine adjustment of Nano-edge filters, which can be confirmed by the transmittance spectra of Nano-edge filters in such geometry.

III. MEASUREMENTS AND DISCUSSION

Now, we apply this ULF Raman system to probe the interface coupling in t(2+2)LGs, which can be prepared by the following two ways. Highly oriented pyrolytic graphite (HOPG) is mechanically exfoliated on a Si/SiO_2 substrate.[26] During the exfoliation, a partial bilayer graphene (BLG) flake is accidentally folded onto the BLG flake itself to form the exfoliated t(2+2)LG (denoted as Ex-t(2+2)LG). Alternatively, a 2LG flake from one substrate can also be transferred onto the 2LG flake on another substrate to form the transferred t(2+2)LG (denoted as Tr-t(2+2)LG). We follow the transfer method described in the literature.[27] The layer number in 2LG and t(2+2)LG is identified by Raman spectroscopy.[28,29]

Nano-edge filters of 488 nm were used to measure Raman spectra of one Ex-t(2+2)LG and one Tr-t(2+2)LG, as shown in Fig. 4(a) along with the corresponding optical images. The intensity of the G mode, I(G), in the two t(2+2)LG is enhanced by the 488 nm excitation in comparison to that in 4 layer graphene (4LG). Based on the observed R modes (~1461 cm^{-1} in Ex-t(2+2)LG and ~1443 cm^{-1} in Tr-t(2+2)LG) and the theoretical results calculated by DFT,[30] the resonant energy for I(G) can be estimated to be 3.0 eV and 3.2 eV for Ex- and Tr-t(2+2)LG, respectively. The 2.54 eV of 488 nm excitation is under the near-resonance condition for the two t(2+2)LGs. Thus, I(G) in Ex- and Tr-t(2+2)LG are slightly enhanced about 2.5 and 1.4 times as strong as that in 4LG, respectively. Both Ex- and Tr-t(2+2)LG exhibit two peaks at ~29 cm^{-1} and 115 cm^{-1}, which are assigned as the C and LB modes, respectively, according to the previous reports on t(m+n)LG.[13,16] The frequency of the LB mode (Pos(LB)) is close to that (116 cm^{-1}) of the LB_{41} mode in estimated by Bernal-stacked 4 layer graphene (4LG) estimated by the linear chain model (LCM),[16] and thus the mode is attributed to the LB_{41} mode in Ex- and Tr-t(2+2)LG. The almost same Pos(LB) between the two t(2+2)LGs and Bernal-stacked 4LG suggests that their interface LB coupling is almost equal to the LB coupling in bulk graphite. However, the Pos(C) in Ex- and Tr-t(2+2)LG is much lower than that (40.3 cm^{-1}) of Bernal-stacked 4LG and is very close to that (30.7 cm^{-1}) of the C_{21} mode in 2LG. This indicates that the interface C coupling in Ex- and Tr-t(2+2)LG is much weaker than that in bulk graphite, as addressed in the previous report.[13,16]

Because the interface C coupling in Ex- and Tr-t(2+2)LG is very weak, there exist two possible normal atomic displacements for the C mode in Ex- and Tr-t(2+2)LG, i.e., in-phase or out-of-phase vibrations between the two interface layers in t(2+2)LG, as demonstrated in Fig. 4(b). The additional van der Waals (vdW) interaction between the two interface layers in the out-of-phase vibrations will raise the frequency of the C mode with respect to the corresponding mode with in-phase vibrations. The frequency difference between the two modes is determined by the vdW interaction between the two interface layers, which is well-known as Davydov splitting in t(2+2)LGs. As Pos(C) in Ex- and Tr-t(2+2)LG is close to Pos(C_{21}) in 2LG, we denote the two C modes with out-of-phase and in-phase vibrations between the two interface layers as C_{21}^{+} and C_{21}^{-}, respectively.

The two C peaks in Ex- and Tr-t(2+2)LG cannot be well-fitted by a Lorentzian peak, indicating that they should consist of two subpeaks related with the Davydov doublets. Indeed, although FWHM(LB_{41}) (6.0 cm^{-1}) of Ex-t(2+2)LG is slightly larger than that (5.3 cm^{-1}) of the previously reported Ex-t(1+3)LG,[16] FWHM(C) (~2.6 cm^{-1}) in Ex- and Tr-t(2+2)LG is much larger than that (~1.4 cm^{-1}) in the previously reported Ex-t(1+3)LG.[13] The dashed lines in Fig. 4(a) reveal the good two-Lorentzian fit to the C peaks in Ex- and Tr-t(2+2)LG. The higher component is assigned as C_{21}^{+} and the lower one C_{21}^{-}. In bulk graphite, the interlayer shear force constant was determined to be $\alpha_0 = 12.8 \times 10^{18}$ Nm^{-3} from Pos(C) (i.e., 43.5 cm^{-1}) in bulk graphite or Pos(C_{21}) (i.e., 30.7 cm^{-1}) in 2LG.[9] Pos(C_{21}^{-}) (29.0 cm^{-1} in Ex-t(2+2)LG, 28.5 cm^{-1} in Tr-t(2+2)LG) is lower than Pos(C_{21}) in 2LG, indicating a softening of the shear force constant (α_{0t}) between layers next to the interface. We obtained α_{0t} of 11.4×10^{18} Nm^{-3} in Ex-t(2+2)LG and 11.0×10^{18} Nm^{-3} in Tr-t(2+2)LG. Then, we can further deduce the force constant (α_t) between the two interface layers from Pos(C_{21}^{+}) based on the LCM where

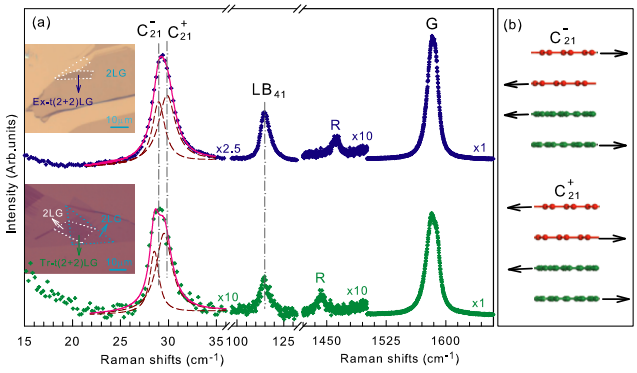

FIG. 4. (a) Raman spectra of exfoliated and transferred t(2+2)LG in the range of the C, LB, and G modes. The insets show the corresponding optical images. The fits show that the C modes are composed of two sub-peaks, C_{21}^{-} and C_{21}^{+}. The spectra are scaled and offset for clarity. (b) Normal mode displacements of the C_{21}^{-} and C_{21}^{+} sub-peaks determined from the linear chain model.

only nearest interlayer coupling is considered.[13] We obtained α_t of 1.9×10^{18} Nm^{-3} in Ex-t(2+2)LG and 1.4×10^{18} Nm^{-3} in Tr-t(2+2)LG, showing that the interface shear coupling is only 11%-15% of the shear coupling in Bernal-stacked layers. Presumably, the different interface couplings in Ex- and Tr-t(2+2)LG may arise from the uncontrollable interlayer distance variation in the process of exfoliation or transferring. Such variation will be very sensitive to peak profile and position of the LB mode. However, the normalized LB modes in Ex- and Tr-t(2+2)LG are almost identical to each other. In fact, this softening has been attributed to the periodicity mismatch between two twisted layers.[16] The twist angle of Ex- and Tr-t(2+2)LG is ~16.8 and ~18.8 determined from the corresponding Pos(R), respectively. The different twist angles could result in different Moiré patterns and different locally mismatched periodicities of the charge density variations. Thus, it is reasonable to exhibit different softening of the interface shear coupling in Ex- and Tr-t(2+2)LG.

IV. CONCLUSIONS

We have demonstrated a ULF Raman system based on a single monochromator with a kind of longpass edge filter. ULF Raman modes can be detected down to 10 cm^{-1} with high throughput and easy operation, which has been verified by measuring ULF modes in Ge/Si quantum dot superlattices and L-cystine. This system has been applied to probe the C modes at 30 cm^{-1} in t(2+2)LG flakes prepared by exfoliation or transferring technique. The shear coupling at twisted interfaces in t(2+2)LG is twist-angle dependent, ~10%-20% of that in bulk graphite, while the layer-breathing coupling at twisted interfaces is almost identical to that in bulk graphite. The former is attributed to the twist-angle dependent periodicity mismatch between two twisted layers. The results show potential application of this Raman system in the research field of ULF Raman spectroscopy.

ACKNOWLEDGMENTS

This work was supported by the National Natural Science Foundation of China, Grant Nos. 11225421, 11434010, 11474277, 21571101, 51522201, and 11474006. H. Li also acknowledges financial support from Specially Appointed Professors by Universities in Jiangsu Province.

[1]V. L. Gurevich, D. A. Parshin, and H. R. Schober, Phys. Rev. B **67**, 094203 (2003).
[2]N. Large, L. Saviot, J. Margueritat, J. Gonzalo, C. N. Afonso, A. Arbouet, P. Langot, A. Mlayah, and J. Aizpurua, Nano Lett. **9**, 3732–3738 (2009).
[3]E. Duval, A. Boukenter, and B. Champagnon, Phys. Rev. Lett. **56**, 2052–2055 (1986).
[4]S. K. Gupta, S. Sahoo, P. K. Jha, A. K. Arora, and Y. M. Azhniuk, J. Appl. Phys. **106**, 024307 (2009).
[5]M. Hu, X. Wang, G. V. Hartland, P. Mulvaney, J. P. Juste, and J. E. Sader, J. Am. Chem. Soc. **125**, 14925–14933 (2003).
[6]H. Lange, M. Mohr, M. Artemyev, U. Woggon, and C. Thomsen, Nano Lett. **8**, 4614–4617 (2008).
[7]P. H. Tan, D. Bougeard, G. Abstreiter, and K. Brunner, Appl. Phys. Lett. **84**, 2632–2634 (2004).
[8]J. Ibáñez, A. Rapaport, C. Boney, R. Oliva, R. Cuscó, A. Bensaoula, and L. Artús, J. Raman Spectrosc. **43**, 237–240 (2012).
[9]P. H. Tan, W. P. Han, W. J. Zhao, Z. H. Wu, K. Chang, H. Wang, Y. F. Wang, N. Bonini, N. Marzari, N. Pugno, G. Savini, A. Lombardo, and A. C. Ferrari, Nat. Mater. **11**, 294–300 (2012).
[10]X. Zhang, W. P. Han, J. B. Wu, S. Milana, Y. Lu, Q. Q. Li, A. C. Ferrari, and P. H. Tan, Phys. Rev. B **87**, 115413 (2013).
[11]X. Zhang, X.-F. Qiao, W. Shi, J.-B. Wu, D.-S. Jiang, and P.-H. Tan, Chem. Soc. Rev. **44**, 2757–2785 (2015).
[12]Y. Zhao, X. Luo, H. Li, J. Zhang, P. T. Araujo, C. K. Gan, J. Wu, H. Zhang, S. Y. Quek, M. S. Dresselhaus, and Q. Xiong, Nano Lett. **13**, 1007–1015 (2013).
[13]J.-B. Wu, X. Zhang, M. Ijäs, W.-P. Han, X.-F. Qiao, X.-L. Li, D.-S. Jiang, A. C. Ferrari, and P.-H. Tan, Nat. Commun. **5**, 5309 (2014).
[14]A. A. Puretzky, L. Liang, X. Li, K. Xiao, K. Wang, M. Mahjouri-Samani, L. Basile, J. C. Idrobo, B. G. Sumpter, V. Meunier, and D. B. Geohegan, ACS Nano **9**, 6333–6342 (2015).
[15]H. Zhao, J.-B. Wu, H. Zhong, Q. Guo, X. Wang, F. Xia, L. Yang, P.-H. Tan, and H. Wang, Nano Res. **8**, 3651–3661 (2015).
[16]J. B. Wu, Z. X. Hu, X. Zhang, W. P. Han, Y. Lu, W. Shi, X. F. Qiao, M. Ijiás, S. Milana, W. Ji, A. C. Ferrari, and P. H. Tan, ACS Nano **9**, 7440–7449 (2015).
[17]X. Zhang, Q.-H. Tan, J.-B. Wu, W. Shi, and P.-H. Tan, Nanoscale **8**, 6435–6450 (2016).
[18]A. A. Puretzky, L. Liang, X. Li, K. Xiao, B. G. Sumpter, V. Meunier, and D. B. Geohegan, ACS Nano **10**, 2736–2744 (2016).
[19]S. Huang, L. Liang, X. Ling, A. A. Puretzky, D. B. Geohegan, B. G. Sumpter, J. Kong, V. Meunier, and M. S. Dresselhaus, Nano Lett. **16**, 1435–1444 (2016).
[20]X. Zhang, W.-P. Han, X.-F. Qiao, Q.-H. Tan, Y.-F. Wang, J. Zhang, and P.-H. Tan, Carbon **99**, 118–122 (2016).
[21]J.-U. Lee, K. Kim, S. Han, G. H. Ryu, Z. Lee, and H. Cheong, ACS Nano **10**, 1948–1953 (2016).
[22]R. He, J.-A. Yan, Z. Yin, Z. Ye, G. Ye, J. Cheng, J. Li, and C. H. Lui, Nano Lett. **16**, 1404–1409 (2016).
[23]X.-F. Qiao, J.-B. Wu, L. Zhou, J. Qiao, W. Shi, T. Chen, X. Zhang, J. Zhang, W. Ji, and P.-H. Tan, Nanoscale **8**, 8324–8332 (2016).
[24]S. G. Belostotskiy, Q. Wang, V. M. Donnelly, D. J. Economou, and N. Sadeghi, Appl. Phys. Lett. **89**, 251503 (2006).
[25]G. Plechinger, S. Heydrich, J. Eroms, D. Weiss, C. Schüller, and T. Korn, Appl. Phys. Lett. **101**, 101906 (2012).
[26]K. S. Novoselov, D. Jiang, F. Schedin, T. J. Booth, V. V. Khotkevich, S. V. Morozov, and A. K. Geim, Proc. Natl. Acad. Sci. U. S. A. **102**, 10451–10453 (2005).
[27]C. R. Dean, A. F. Young, I. Meric, C. Lee, L. Wang, S. Sorgenfrei, K. Watanabe, T. Taniguchi, P. Kim, K. L. Shepard, and J. Hone, Nat. Nanotechnol. **5**, 722–726 (2010).
[28]W.-J. Zhao, P.-H. Tan, J. Zhang, and J. Liu, Phys. Rev. B **82**, 245423 (2010).
[29]X.-L. Li, X.-F. Qiao, W.-P. Han, Y. Lu, Q.-H. Tan, X.-L. Liu, and P.-H. Tan, Nanoscale **7**, 8135–8141 (2015).
[30]V. Carozo, C. M. Almeida, B. Fragneaud, P. M. Bedê, M. V. O. Moutinho, J. Ribeiro-Soares, N. F. Andrade, A. G. Souza Filho, M. J. S. Matos, B. Wang, M. Terrones, R. B. Capaz, A. Jorio, C. A. Achete, and L. G. Cançado, Phys. Rev. B **88**, 085401 (2013).